Role of surface roughness characterized by fractal geometry on laminar flow in microchannels

Yongping Chen,[1,*] Chengbin Zhang,[1] Mingheng Shi,[1] and G. P. Peterson[2]
[1]*School of Energy and Environment, Southeast University, Nanjing, Jiangsu 210096, People's Republic of China*
[2]*Office of the President, Georgia Institute of Technology, Atlanta, Georgia 30332-0325, USA*
(Received 14 February 2009; published 5 August 2009)

A three-dimensional model of laminar flow in microchannels is numerically analyzed incorporating surface roughness effects as characterized by fractal geometry. The Weierstrass-Mandelbrot function is proposed to characterize the multiscale self-affine roughness. The effects of Reynolds number, relative roughness, and fractal dimension on laminar flow are all investigated and discussed. The results indicate that unlike flow in smooth microchannels, the Poiseuille number in rough microchannels increases linearly with the Reynolds number, Re, and is larger than what is typically observed in smooth channels. For these situations, the flow over surfaces with high relative roughness induces recirculation and flow separation, which play an important role in single-phase pressure drop. More specifically, surfaces with the larger fractal dimensions yield more frequent variations in the surface profile, which result in a significantly larger incremental pressure loss, even though at the same relative roughness. The accuracy of the predicted Poiseuille number as calculated by the present model is verified using experimental data available in the literature.

DOI: 10.1103/PhysRevE.80.026301 PACS number(s): 47.15.−x, 47.53.+n, 07.10.Cm

I. INTRODUCTION

In classical fluid mechanics, the wall roughness is typically considered negligible for laminar flow. However, with decreasing channel size and increasing relative roughness, as applied in MEMS devices, the wall roughness increases in importance. An important question whether or not there is effect of roughness on laminar internal flow has been asked repeatedly in more recent studies [1].

In spite of a large number of studies of fluid flow and heat transfer characteristics in microchannels, considerable great differences still exist between the available experimental data [2–7]. While some of these variations may be the result of measurement error, differences in the channel surface conditions, especially differences in the channel roughness [1], may be the dominant reason. When considering mini/microchannels ($10\ \mu m \leq d_h \leq 3$ mm) [8], the ratio between the geometry of the roughness profile and the hydraulic diameter becomes significantly different from what typically occurs in more conventional channels. At this scale, the shape, spacing, and size of the roughness irregularities have a very different influence upon the pressure drop and the overall fluid flow characteristics. For this reason, the role of surface roughness on the liquid flow in microchannels has become increasingly important and of considerable interest in the past several years.

Pfund *et al.* [9] measured the friction factors in rough rectangular microchannels with depths ranging from 128 μm to 521 μm. The results of this investigation indicated significant differences between the experimental results observed and classical theory. Hu *et al.* [10] developed a three-dimensional finite volume based numerical model to simulate pressure driven liquid flow in microchannels with rectangular prism rough elements on the surface. In this investigation, the effects of surface roughness in terms of the rough elements' height, size, spacing, and the channel height on both the velocity distribution and pressure drop were examined and found to be significant. Croce and Agaro [11,12] investigated the roughness effect on the heat transfer and pressure loss in microscale channels through a finite element CFD code. The surface roughness was explicitly modeled through a set of random generated peaks along an ideal smooth surface.

Kleinstreuer and Koo [13] proposed a computational model to consider the effects of wall roughness on liquid flow in microchannels. The roughness layer was modeled as a porous medium near the wall. This model has been found to be of particular utility at very low Reynolds numbers, with very high relative roughness. Bahrami *et al.* [14] developed an analytical model to predict the pressure drop of fully developed, laminar, incompressible flow in rough microtubes, in which the roughness was assumed to be subjected to GAUSSIAN distribution. Taylor *et al.* [15] laid out the historical and current understanding of the effects of surface roughness and texture on fluid flow, and explored several potential methods for improving the understanding of and controlling the effect of surface roughness and texture.

To investigate the mechanisms of flow in rough microchannels, it is necessary to quantify the relative roughness. One way in which this can be accomplished is through a set of roughness descriptors suitable for microchannels and minichannels. This would provide a mechanism by which the effects of different aspects of the surface topography upon the pressure drop and fluid flow behavior can be quantified [15,16]. There have been several previous attempts to utilize this approach, including the use of randomly generated peaks [12], porous media [13], and GAUSSIAN distributions [14] to describe the surface roughness (see Fig. 1). However, the rough surface topography is a nonstationary random process and the scan values of roughness by instruments with different resolutions and scan lengths can be very different for the same surface [17]. The above three approaches are still constructed on statistical mean and difficult to absolutely characterize the exact nature of such multiscale and random

*Corresponding author; ypchen@seu.edu.cn

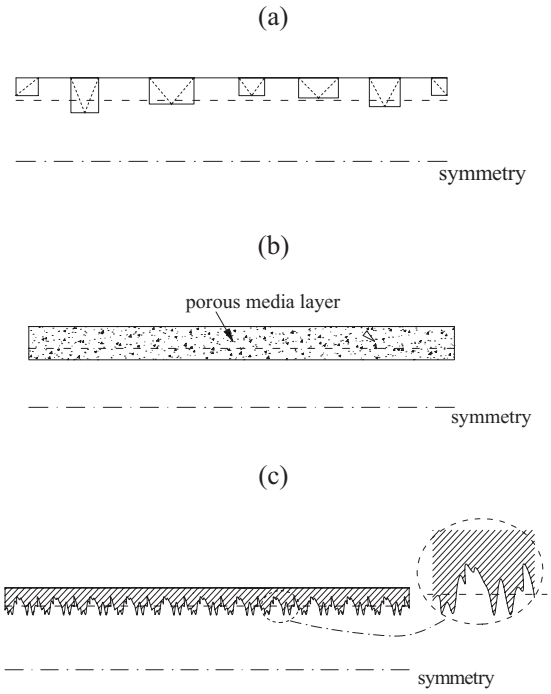

FIG. 1. Construct of microchannel surface roughness available in the literature: (a) roughness modeled through random peaks [12], (b) roughness modeled as porous medium [13], (c) roughness subjected to GAUSSIAN distribution [14].

rough surface. As a result, a proper scale-invariant characterization of the rough surface topography must be developed.

In this paper, inspired by the successful utilization of fractal geometry in exploring the role of roughness on friction and wear of sliding solid surfaces [18–22], the fractal geometry is introduced to characterize the microchannel surface profile and to determine its impact on laminar flow in rough microchannels. A three-dimensional model of laminar fluid flow in microchannel with fractal rough surfaces is developed and analyzed numerically. The effects of Reynolds number, relative roughness, and self-affine fractal dimension on the laminar flow are all investigated and discussed. In addition, the accuracy of the Poiseuille number as determined by the present model is verified using experimental data available in the literature.

II. FRACTAL CHARACTERIZATION OF ROUGH SURFACES

Fractal geometry was founded by Mandelbrot [23–25] to describe disordered objects using fractal dimensions. Differing from Euclidean geometry, fractal geometry suggests that the dimensions of the disordered and irregular objects such as a natural coastlines [23], fractal trees [26,27], porous media [28], and rough surfaces [22] can all be noninteger related.

It is well documented that, as shown in Fig. 2, when a surface is magnified appropriately, the magnified image looks very similar to the original profile, i.e., the roughness at all magnifications appear quite qualitatively similar in structure [18]. These rough surface profiles nearly always

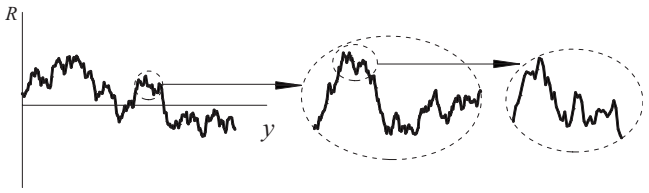

FIG. 2. Qualitative description of statistical self-affinity for a surface profile.

follow power laws and hence create a self-affine property. By using a more general class of fractals, the so-called self-affine fractals, characterization of surface roughness from the nanometer to the millimeter scale has been demonstrated [18,22]. The profile of a surface, $R(y)$, can be assumed to be continuous down to an infinitesimal of length scale by neglecting the discrete atomic arrangement. The continuity, self-affinity and nondifferentiability of the surface profile are preserved by a fractal characterization, in which $R(y)$ is represented by the Weierstrass-Mandelbrot (W-M) function [22],

$$R(y) = G^{(D-1)} \sum_{n=n_1}^{\infty} \frac{\cos(2\pi\gamma^n y)}{\gamma^{(2-D)n}}; \quad 1 < D < 2; \quad \gamma > 1 \tag{1}$$

where, G is a scaling constant, D is the self-affine fractal dimension, G and D are independent of the resolution of the scan instruments and scale, γ is the scaling parameter for determining the spectral density and self property. In the roughness investigation, $\gamma = 1.5$ is shown to be a suitable value [22]. The parameter, n_1, is used to specify the low cut-off frequency in the W-M function. This parameter is numerically related to the sample length, L_s by $\gamma^{n1} = 1/L_s$.

The Weierstrass-Mandelbrot function, $R(y)$, is a multiscale function, composed of a superposition of infinite frequency modes. The power spectrum of this multiscale function can be described as

$$s(\omega) = \frac{G^{2(D-1)}}{2 \ln \gamma} \frac{1}{\omega^{(5-2D)}}. \tag{2}$$

The structure function, $\mathrm{Str}(\tau)$

$$\mathrm{Str}(\tau) = \langle [R(y+\tau) - R(y)]^2 \rangle = \int_{-\infty}^{\infty} s(\omega)(e^{i\omega\tau} - 1) d\omega = \psi G^{2(D-1)} \tau^{(4-2D)} \tag{3}$$

where, $\langle\ \rangle$ implies temporal average, ψ is a constant,

$$\psi = \frac{\Gamma(2D-3)\sin[(2D-3)\pi/2]}{2 \ln \gamma (2-D)}. \tag{4}$$

The root-mean-square (rms) roughness height

$$\sigma = \langle R^2 \rangle^{0.5} = \left[\int_{\omega_l}^{\omega_h} s(\omega) d\omega \right]^{0.5} = \left[\frac{G^{2(D-1)}}{2 \ln \gamma} \frac{1}{4-2D} \left(\frac{1}{\omega_l^{(4-2D)}} - \frac{1}{\omega_h^{(4-2D)}} \right) \right]^{0.5} \quad (5)$$

where, τ is the scale, the low cut-off frequency, ω_l, is provided by the sample length as $\omega_l = 1/L_s$, and the high-frequency limit, ω_h, is related with the resolution of scan instrument, L_r, as $\omega_h = 1/L_r$.

The fractal nature of a real surface profile can be verified either by finding its power spectrum and then comparing it with Eq. (2) or by calculating its structure function to see if it satisfies the relationship given in Eq. (3) [29]. In the current study, the self-affine fractal dimension is calculated by structure function.

By plotting $\mathrm{Str}(\tau)$ as a function of the scale τ on a log-log plot, the relationship between the log $\mathrm{Str}(\tau)$ and the log τ can be observed to determine if it satisfies the proportional relationship as $\mathrm{Str}(\tau) \sim \tau^{(4-2D)}$. If this proportional relationship is satisfied, the roughness is a self-affine fractal object and the self-affine dimension $D = (4-k)/2$, in which k is the slope of the structure function.

Once a sample of real surface topography is given, the self-affine fractal dimension, D, can be determined by the above method, and the scaling constant, G, can be obtained by introducing the rms value scanned by profilometer into Eq. (5). Therefore, once D, which implies the irregularity of surface roughness, and σ, which describes the statistical mean height of roughness are determined, a more realistic characterization of rough surface based on Eq. (1) can be specified.

In order to give a clearer understanding of self-affine roughness, the surface profiles for different self-affine fractal dimensions, but the same rms roughness heights as constructed on the self-affine law by the Weierstrass-Mandelbrot function, Eq. (1), are plotted in Fig. 3. As shown, although the rms roughness heights are the same for these profiles, the distributions of roughness are clearly different. The roughness profile with the larger self-affine fractal dimension, yields more frequent variations along the profile. This is apparent in the figure, where the self-affine fractal dimension, D, can directly exhibit the irregularity of the surface profile. In this comparison, it is also implied that D and σ are independent parameters.

Channel surfaces (see Fig. 4) suggested by Pfund *et al.* [9] are examined in this investigation. The self-affine fractal dimensions for these channel surfaces are plotted in Fig. 5. The nearly straight line of the structure function on a log-log plot suggests that the power-law behavior of Eq. (3) is satisfied. Thus, these channel surfaces are self-affine fractal object and the roughness can be realistically characterized by Eq. (1).

III. LAMINAR FLOW IN ROUGH MICROCHANNELS

A. Mathematical model

In order to analyze the influence of surface roughness on laminar flow in microchannel, the laminar flow in rectangular microchannels with large width/span ratios as shown in Fig. 6 is investigated as an example. In order to simplify the calculation, only the rough profile on top and bottom surfaces along the y direction is considered, and the two sides is selected as smooth surface. The W-M function, $R(y)$, is applied to characterize the rough surface, and the different rough profile can be acquired by adjusting parameters D and G in Eq. (1).

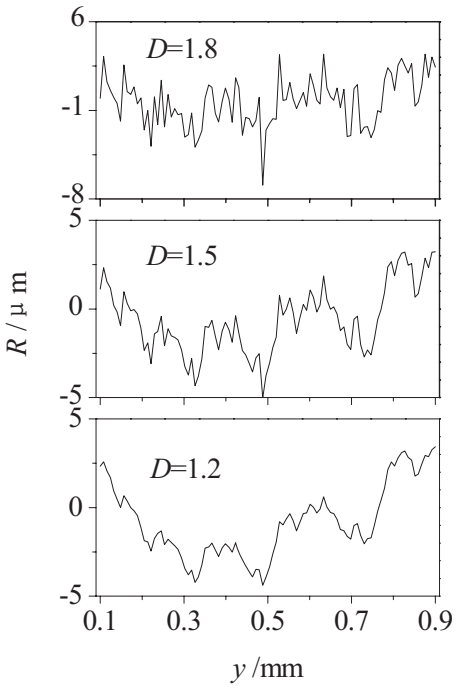

FIG. 3. Simulated fractal surface profile ($\sigma = 2$ μm).

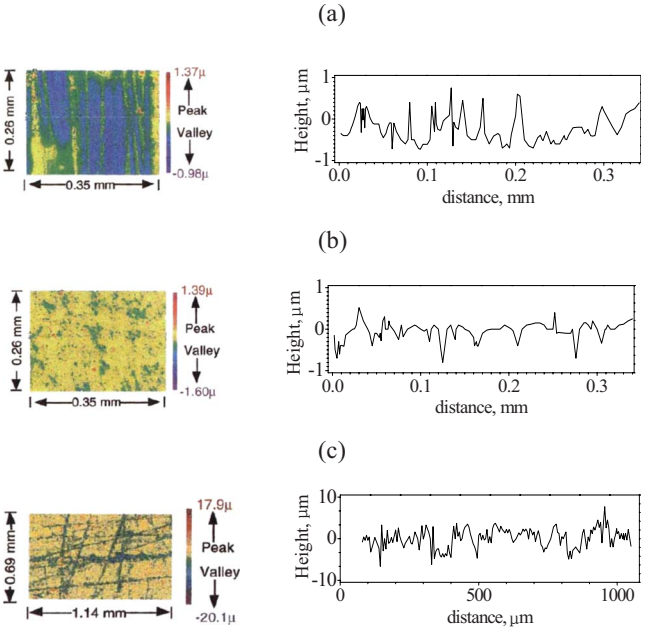

FIG. 4. (Color online) Profilometer images of channel surfaces [9]: (a) top plate, (b) smoother polyimide bottom plate, (c) rough polyimide bottom plate.

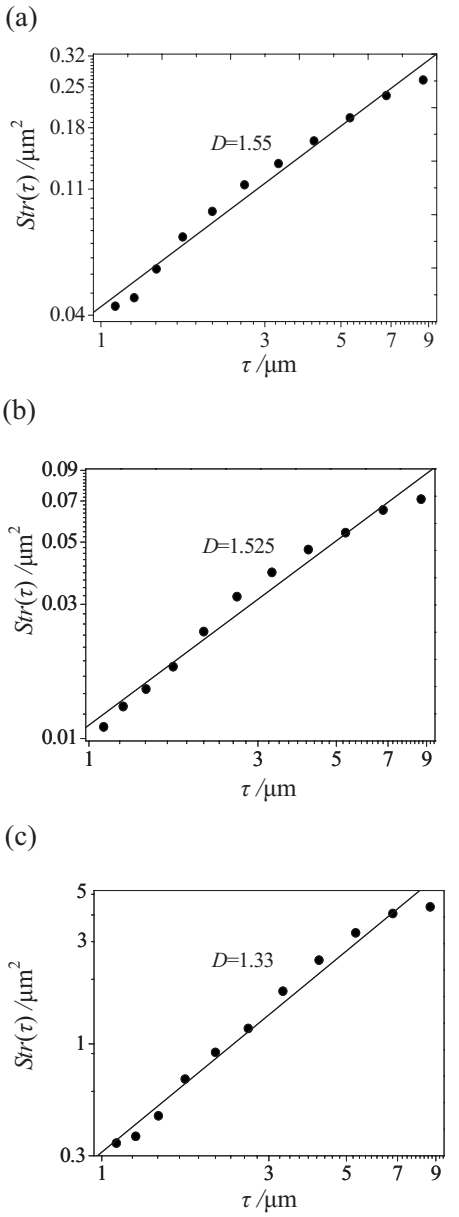

FIG. 5. Plot of $\mathrm{Str}(\tau) \sim \tau$ of surface roughness for polyimide channel: (a) top plate, (b) smoother polyimide bottom plate, (c) rough polyimide bottom plate.

The following assumptions are applied to the model:
(1) steady laminar flow;
(2) constant fluid properties;
(3) negligible gravity.

While initially there was some question, it has been previously confirmed that the Navier-Stokes equations are still valid for laminar flow in microchannels [6,7]. Thus, the momentum and continuity equations for laminar flow in rough microchannels still can be presented as

$$\rho(\vec{V} \cdot \nabla \vec{V}) = -\nabla P + \mu \nabla^2 \vec{V} \tag{6}$$

$$\nabla \cdot \vec{V} = 0 \tag{7}$$

where, P is the fluid pressure, ρ is the fluid density, μ is the fluid viscosity, and $\vec{V}$ is the velocity of the fluid.

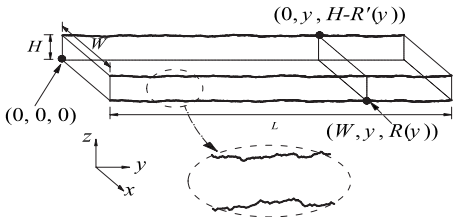

FIG. 6. Schematic of microchannel with rough surface.

The boundary condition of the fluid velocity at the channel inlet is

$$y = 0: \quad u = 0, \quad v = v_{in}, \quad w = 0 \tag{8}$$

where, v_{in} is the given fluid velocity at the channel inlet, u, v, and w are the components of the velocity vector along the x, y, and z directions, respectively. By considering of the fully developed flow at the channel outlet, the outlet boundary condition can be written as

$$y = L: \quad \frac{\partial u}{\partial y} = 0, \quad \frac{\partial v}{\partial y} = 0, \quad \frac{\partial w}{\partial y} = 0. \tag{9}$$

Applying a no-slip boundary condition, the velocity on the wall is

$$\vec{V} = 0: \quad \begin{cases} z = H - R'(y) \\ z = R(y) \\ x = 0 \\ x = W \end{cases} . \tag{10}$$

In general, the laminar internal flow is characterized by Poiseuille number (friction constant), which is

$$\mathrm{Po} = \overline{f\,\mathrm{Re}} = \frac{1}{L - L_e} \int_{L_e}^{L} f(y)\mathrm{Re}(y)dy \tag{11}$$

where, f is the friction factor, L_e is the entrance length, and L_e/H is approximately 0.053 Re for internal laminar flow [30]. In the current study, ε is defined as the ratio of the rms roughness height, σ, to the hydraulic diameter of the microchannel, d_h, $\varepsilon = \sigma / d_h$

B. Numerical method

The numerical solution of Eqs. (6) and (7) for the velocity and pressure fields in rough microchannels is obtained by means of the control volume finite-difference technique and the SIMPLE algorithm [31]. For the complex rough surface evaluated and shown in Fig. 6, a structured mesh based on hexahedron grid elements is applied to arrive at a solution. A nonuniform grid arrangement along the y direction with a large number of grid points near the channel inlet is used to resolve the flow developing region and the nonuniform gird in cross section is also arranged to resolve fluid flow with consideration of the effect of the boundary layer flow. The resulting system of algebraic equations is solved using the Gauss-Seidal iterative technique, with successive over-relaxation to improve the convergence time.

The numerical code is verified in a number of ways to ensure the validity of the numerical analysis. A grid indepen-

TABLE I. Data for the flow in polyimide microchannels

Size of cross-sections[a]		Channel No. 1 ($H=521$ μm, $W=1$ cm)	Channel No. 2 ($H=263$ μm, $W=1$ cm)	Channel No. 3 ($H=257$ μm, $W=1$ cm)
D (top)[b]		1.55	1.55	1.55
D (bottom)[b]		1.525	1.525	1.33
σ (top) /μm [c]		0.44	0.44	0.44
σ (bottom) /μm [c]		0.20	0.20	2.16
Po	Numerical[d]	24.1	24.9	27.0
	Classical[a]	22.4	23.2	23.2
	Experimental[a]	24.2 ± 1.3	26.1 ± 2.3	29 ± 2.4

[a]Data is obtained from Reference [9].
[b]Values are determined from Fig. 5.
[c]Values are determined from Fig. 4.
[d]Values are calculated with the mean value of Re in laminar experiment [9], i.e., Re is 1300, 1000, and 1100 for channel numbers 1, 2 and 3, respectively.

dence test is conducted using several different mesh sizes. This test proved that the results based on the final grid system presented in this paper are independent of the mesh size. In addition, the solution is regarded as convergent not only by examining residual levels of velocity below 10^{-6}, but also by monitoring relevant integrated quantities and checking for mass balances.

C. Case validation

Laminar flow in rough microchannels with large width/span ratios (#1, 19.2; #2, 38.2; #3, 38.9) suggested by Pfund *et al.* [9] is simulated in this investigation, which to give a verification of the present model. Table I presents the parameters for the flow in these polyimide microchannels. In particular, the calculated Po is compared with that measured experimentally [9]. As shown in the table, the calculated Po in the present paper agrees with the experimental value within the uncertainty. This good agreement between the numerical results and the experimental data verifies the present model is reasonable.

IV. ROLE OF ROUGHNESS ON LAMINAR FLOW

The presence of roughness leads to a change of velocity profile for laminar flow in microchannel, which plays considerable role on the pressure drop along the channel. Figure 7 compares the water flow pressure drop along the smooth and rough microchannel. As shown in the figure, the pressure drop in the rough channel is larger than that in the smooth channel and a rough surface with a higher fractal dimension results in a higher pressure drop. The fluctuation characteristic of pressure drop due to the vortex generated at the roughness can also be found in the figure.

In order to give a clearer understanding of the effect of roughness on fluid flow, an example of two-dimensional local near-wall streamlines, especially the visualization of the vortex in the valley of roughness, is illustrated in Fig. 8, and the effect of vortex formation on pressure drop for this local section is given in Fig. 9. As shown in the figures, the peaks and valleys of rough surface obviously perturb the local flow, and swirl patterns are observed near the channel walls. In addition, the pressure gradient at the location of vortex formation (see ①–⑦ in Figs. 8 and 9) is significantly larger than that in no vortex region. This phenomenon implies that the presence of rough elements results in a counterpressure distribution near the surface and consequently leads to an increase of friction factor for laminar flow.

Figure 10 compares the Poiseuille number as a function of Re for different depth/width ratios in the channel. Differing from the smooth microchannels, Poiseuille number of rough microchannels is no longer constant with Re, but rather increases linearly with Re and is larger than the classical value.

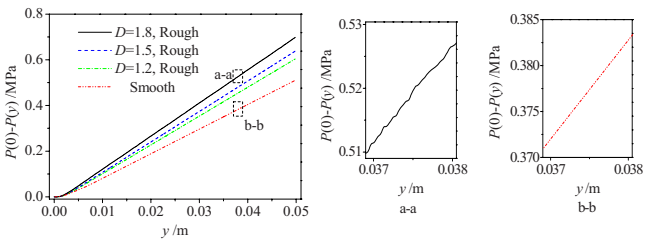

FIG. 7. (Color online) Pressure drop in channels ($W=1$ mm, $H=100$ μm, $L=0.05$ m, $\varepsilon=1\%$, Re=1500).

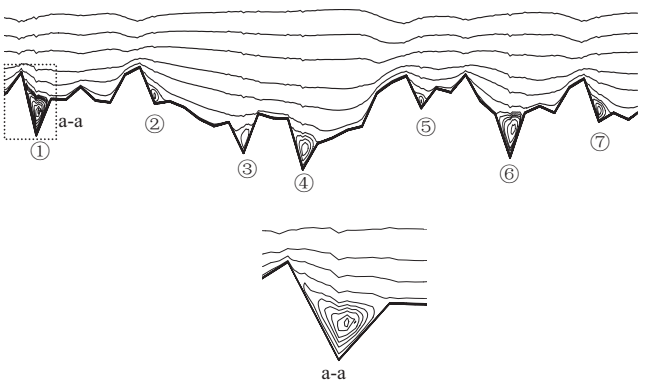

FIG. 8. Local streamlines in the near-wall region ($H=100$ μm, Re=1500, $D=1.8$, $\varepsilon=2\%$).

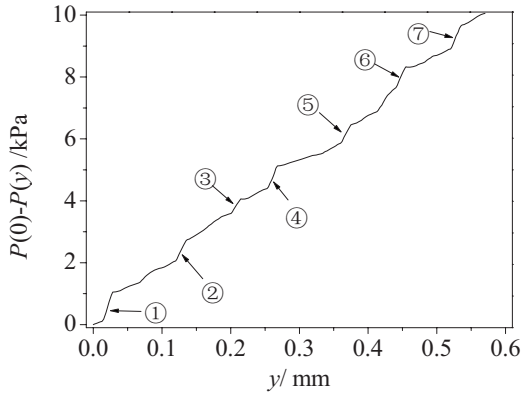

FIG. 9. Effect of vortex formation on pressure drop.

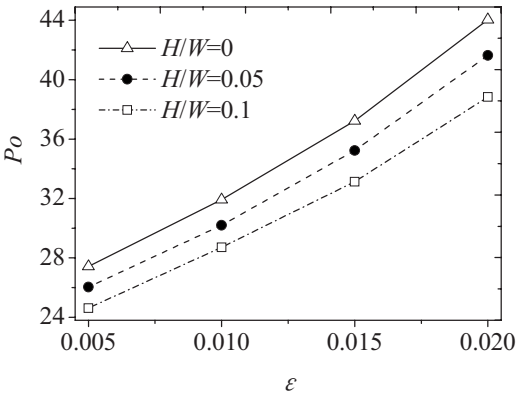

FIG. 11. Effect of ε on Po ($D=1.8$, Re$=1500$).

This phenomenon implies that the vortex effects become more and more important with the increasing Re in rough microchannels. In other words, the vortex effects contributed by the roughness at lower Re is much smaller than that at larger Re, therefore, the Poiseuille number at lower Re is a little higher than the classical value, but differing from the classical value more and more with the increasing Re.

Figure 11 illustrates the effect of relative roughness, ε, on Po. As shown in the figure, at the same fractal dimension, the Poiseuille number increases in a nearly linear fashion with ε. In particular, for high values of relative roughness, the flow over rough features induces recirculation and flow separation, which contributes to an increase in the single-phase pressure drop.

In addition, as shown in Fig. 12, even for surfaces with the same relative roughness, the value of Po is influenced by the roughness irregularities, as indicated by the fractal dimension, D. Since roughness with larger self-affine fractal dimensions yields more frequent variations on the surface profile, this results in a significantly larger increment in pressure losses.

Therefore, the Poiseuille number for laminar flow in microchannels of a specific cross-sectional shape with a rough surface is a function of the Reynolds number, Re, the ratio of the wall roughness height to the hydraulic diameter, ε, and the self-affine fractal dimension, D.

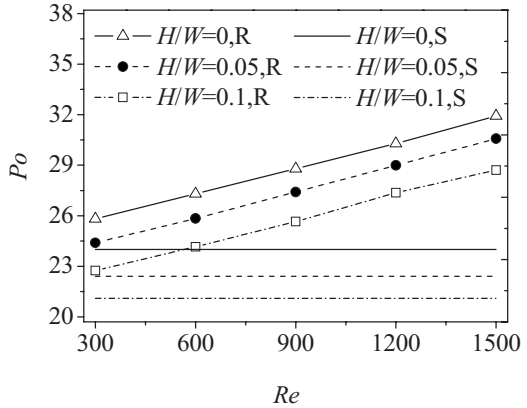

FIG. 10. Effect of Re on Po (R-rough, $D=1.8$, $\varepsilon=1\%$; S-smooth classical).

V. CONCLUSIONS

A three-dimensional model of laminar fluid flow in microchannels with fractal rough surfaces is developed and analyzed numerically. The W-M function is introduced to characterize the roughness. The effect of Reynolds number, relative roughness, and the self-affine fractal dimension on laminar flow are all investigated and discussed. In addition, the accuracy of the calculated Poiseuille number as determined by the present model is verified using experimental data available in the literature. The conclusions can be summarized as follows:

(1) The rough surface can be characterized by the fractal geometry, which utilizes the self-affine fractal dimension to indicate the irregularity of a surface profile. For two profiles with the same mean relative roughness, the fractal dimension may be different.

(2) Differing from the classical theory, the Poiseuille number of rough microchannels is no longer constant with Re, but increases linearly with Re and is larger than the classical value. The vortex effect contributed by the roughness turns to be more and more important with the increasing Re.

(3) With increasing relative roughness, the flow over rough features induces more recirculation and flow

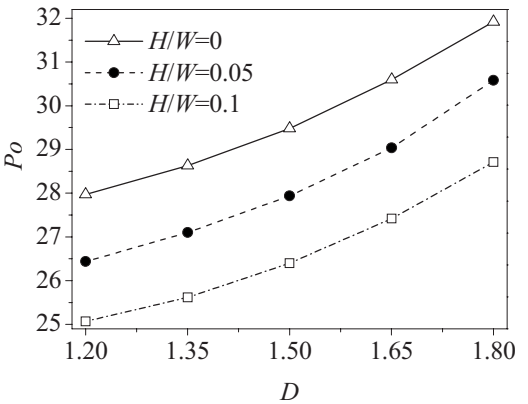

FIG. 12. Effect of D on Po ($\varepsilon=1\%$, Re$=1500$).

separation, which contributes to an increasing single-phase pressure drop.

(4) Surfaces with larger self-affine fractal dimensions, yield more frequent variations in the surface profile and also result in a significantly larger increment in pressure losses.

ACKNOWLEDGMENT

The authors gratefully acknowledge the support provided by National Natural Science Foundation of China (Grant No.50806012).

[1] S. G. Kandlikar, Nanoscale Microscale Thermophys. Eng. **12**, 61 (2008).
[2] D. B. Tuckerman and R. F. W. Pease, IEEE Electron Device Lett. **ELD-2**, 126 (1981).
[3] X. F. Peng and G. P. Peterson, Int. J. Heat Mass Transfer **39**, 2599 (1996).
[4] Z. X. Li, D. X. Du, and Z. Y. Guo, Microscale Thermophys. Eng. **7**, 253 (2003).
[5] M. M. Rahman, Int. Commun. Heat Mass Transfer **27**, 495 (2000).
[6] W. L. Qu, G. M. Mala, and D. Q. Li, Int. J. Heat Mass Transfer **43**, 3925 (2000).
[7] G. D. Wang, L. Hao, and P. Cheng, Int. J. Heat Mass Transfer **52**, 1070 (2009).
[8] S. G. Kandlikar and W. J. Grande, *First International Conference Microchannels and Minichannels* (Rochester, New York, 2003).
[9] D. Pfund, D. Rector, and A. Shekarriz, AIChE J. **46**, 1496 (2000).
[10] Y. D. Hu, C. Werner, and D. Q. Li, ASME J. Fluids Eng. **125**, 871 (2003).
[11] G. Croce and P. D'Agaro, J. Phys. D **38**, 1518 (2005).
[12] G. Croce and P. D'Agaro, Superlattices Microstruct. **35**, 601 (2004).
[13] C. Kleinstreuer and J. Koo, ASME J. Fluids Eng. **126**, 1 (2004).
[14] M. Bahrami, M. M. Yovanovich, and J. R. Culham, ASME J. Fluids Eng. **128**, 632 (2006).
[15] J. B. Taylor, A. L. Carrano, and S. G. Kandlikar, Int. J. Therm. Sci. **45**, 962 (2006).
[16] S. G. Kandlikar, D. Schmitt, A. L. Carrano, and J. B. Taylor, Phys. Fluids **17**, 100606 (2005).
[17] R. S. Sayles and T. R. Thomas, Nature **271**, 431 (1978).
[18] A. Majumdar and B. Bhushan, ASME J. Tribol. **113**, 1 (1991).
[19] S. Wang and K. Komvopoulos, ASME J. Tribol. **116**, 812 (1994).
[20] S. Wang and K. Komvopoulos, ASME J. Tribol. **116**, 824 (1994).
[21] A. Majumdar and B. Bhushan, ASME J. Tribol. **112**, 205 (1990).
[22] A. Majumdar and C. L. Tien, Wear **136**, 313 (1990).
[23] B. B. Mandelbrot, Science **156**, 636 (1967).
[24] B. B. Mandelbrot, Proc. Natl. Acad. Sci. U.S.A. **72**, 3825 (1975).
[25] B. B. Mandelbrot, *The fractal geometry of nature* (Freeman, New York, 1983).
[26] A. Bejan and S. Lorente, J. Appl. Phys. **100**, 041301 (2006).
[27] Y. P. Chen and P. Cheng, Int. J. Heat Mass Transfer **45**, 2643 (2002).
[28] B. M. Yu, Appl. Mech. Rev. **61**, 050801 (2008).
[29] A. Majumdar and C. L. Tien, ASME J. Heat Transfer **113**, 516 (1991).
[30] R. Y. Chen, J. Fluids Eng. **95**, 153 (1973).
[31] S. V. Patankar, *Numerical heat transfer and fluid flow* (Hemisphere, Washington, DC, 1980).